Liquid refractive index sensor based on polymer fiber with micro-holes created by femtosecond laser

Wenchao Dong (董文超), Jue Wei (韦 珏), Xuehai Wang (王学海), Zhihui Kang (康智慧), and Xiaofeng Xu (徐晓峰)*

College of Physics, Jilin University, Changchun 130012, China

**Corresponding author: xuxf@jlu.edu.cn.*

Received March 12, 2014; accepted May 20, 2014; posted online August 8, 2014

We present a liquid refractive index (RI) sensor based on step-index multimode polymer optical fiber with a micro-hole drilled by the femtosecond laser. The experimental results show that in the RI operation range of 1.333–1.473, the sensor has a good linear loss (dB) response to the liquid RI in the micro-holes and a high sensitivity of 18 dB/RIU approximately. The experimental results are explained with the mode of the refraction loss caused by the hole–core interface and connection loss caused by the gap of the holes. The sensor has many advantages including high sensitivity and low cost.

OCIS codes: 060.2370, 060.2310, 060.2300.

doi: 10.3788/COL201412.090601.

Optical fiber sensors have attracted considerable interests and many applications in various areas[1–3]. One of them is in a high-precision continuous liquid refractive index (RI) measurement[4], which is the key to environmental monitoring, medical diagnosis, and other biochemical detection technology. Such technology possesses a variety of advantages including resistance to electromagnetic interference, electrical insulating and corrosion resistance properties, distant measuring, etc[5].

Silica fiber sensors, such as fiber Bragg grating (FBG) sensors, long-period fiber grating (LPFG) sensors, surface plasma resonance (SPR) sensors, and Fabry-Perot (F-P) or micro-hole fiber sensors, have been widely used to measure the RI of ambient media and demonstrated high sensitivity. Even then, there are still some problems that are difficult to overcome. FBG sensors based on D-shaped fiber[6,7] have weak strength and poor durability because of the removal of the fiber cladding. LPFG sensors have a high sensitivity to the RI of the ambient media but the multiple resonance peaks and broad transmission resonance features may constrain its measurement accuracy[8–10]. Silica fiber sensors based on SPR have difficulties in coating a sufficiently thin film to a high quality on a fiber. Silica fiber RI sensors based on F-P or micro-hole[11–16] are affected by having a small RI range and a nonlinear response to the RI variation, and materials are also expensive .

Besides silica fiber sensors, the polymer optical fiber (POF) sensors have also undergone significant development in the past years[17,18]. The main advantages of plastic fiber sensors are their ease of handling, mechanical strength, disposability and easy mass production of components and system. Furthermore, the POF-based sensors do not require sophisticated material, it can be easily automated and operated at room temperature and varying pressure conditions. The sensing mechanism of the POF sensors is done by changing the ambient media around the fiber cladding which leads to the changes in the output power of the fiber, and then the ambient variation can be measured according to the output power[17,19,20].

We present a kind of plastic optical fiber sensor fabricated by femtosecond laser. Femtosecond laser is proven to be an efficient micromachining tool to fabricate many silica fiber sensor devices. For example, femtosecond laser has been used for the inscription of FBGs[21] and the fabrication of microcavity fiber-optic sensors[22,23]. Femtosecond laser can also be used for the micromachining of plastic optical fiber sensors. Here another kind of POF sensor with a micro-hole created by femtosecond laser is proposed and demonstrated. The sensitivity and linearity range of the sensors are investigated with different micro-hole diameters. The advantages of this kind of POF sensor are high sensitivity, good linearity, large measurement range, low-temperature sensitivity, and low-processing cost. It is very important for biomedical, chemical, and environmental monitoring applications as well.

The micro-hole inscription into the fiber was used by a tightly focused femtosecond laser beam. Light pulses generated by a regeneratively amplified, titanium-sapphire laser (center wavelength of 800 nm) were focused into the POF by using a lens, with a focal length of 20 mm. The laser pulse width was about 110 fs, and the repetition rate was 1 kHz. The laser energy used for fabrication was about 0.5 mJ per pulse. In order to investigate the influence of different micro-holes, different diameters were drilled. The fiber was mounted on a three-dimensional mobile platform, so that the micro-holes could be fabricated on the core of the fibers and that the desired structure of the micro-holes could be inscribed by adjusting it. The aperture sizes of the

micro-holes drilled by the laser pulse in the fiber were measured about 0.32, 0.44, and 0.64 mm.

After the laser inscription process, we measured the sensitivity and linearity of the fiber-optic sensors with different micro-hole diameters. The relative schematic diagram is shown in Fig. 1. The simple fiber sensor mainly consisted of 650 nm semiconductor laser, the fiber sensor head, light detection module, and a function generator which was used to modulate the semiconductor laser. The light detection module, which was composed of a photoelectric converter and an oscilloscope, converted optical signals into electrical signals and then displayed it in the form of voltage. As shown, the sensing head was fixed on the fiber fixing device to protect the hole from shaking or bending and to avoid any unnecessary error. The modulated light emitted by the semiconductor laser was coupled to the fiber sensor, and the ambient variation could be known by detecting the fiber output power. During the test, the hole in the fiber was filled by an injector with a series of RI liquid samples comprising glycerin–water mixture. Before each measurement, the sensing head was cleaned carefully for a few minutes by using an ultrasonic cleaner so that there was no residual liquid or any other contaminant left inside the hole.

To investigate the RI response, the RI measurements of the proposed sensors with different micro-hole diameters were carried out. In Fig. 2, the losses of the sensors with 0.32, 0.44, and 0.64 mm diameters, respectively, are plotted as a function of n_h which is the RI of the glycerin–water mixtures in the holes. The incident power of the sensing fiber was 12.3 dBm. Measurements were performed five times at each RI value. Fluctuations in the range of measured value were less than 0.002 dB. And the largest difference among the five measurements was 0.18%. As shown, the sensors revealed a large operation range of 1.333–1.473, a good linear dB response to the RI and a sensitivity of 18 dB/RIU approximately. It can also be found that the relationship between the fiber loss and the RI in the holes is dependent on the micro-hole diameter and the sensitivity of the sensors increases with the aperture of the holes. The response of the sensors can be explained

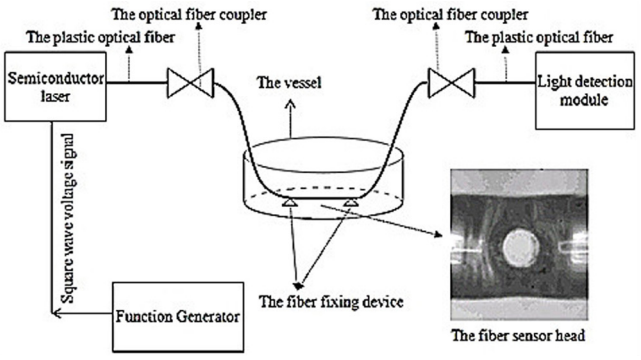

Fig. 1. Experiment setup of fiber-optic liquid RI sensor and the top view of the fiber sensor head in CCD corresponding to the micro-hole of 0.64 mm diameter.

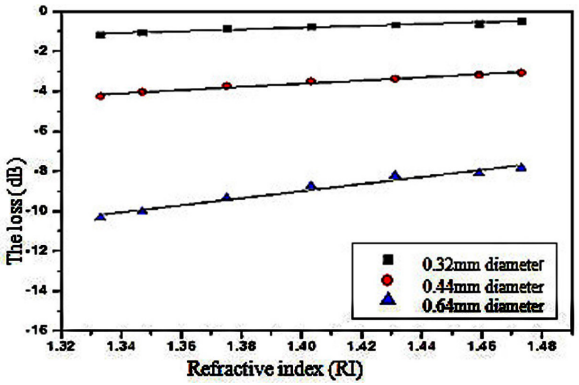

Fig. 2. Loss of the fiber-optic sensors against the RI in the holes for different diameters of the micro-holes.

with the modeling of the refraction loss caused by the hole–core interface and connection loss caused by the gap of the holes. We assumed that the transmission power in the fiber cross-section was of uniform distribution, and the reflected light power at the hole–core interface was neglected. Furthermore, we only discussed the loss of the fiber sensors caused by the meridional rays running parallel to the axis and neglected the rays having other incident angle.

We first analyze the refraction loss of the fiber sensors caused by the hole–core interface. For convenience, the micro-hole in the fiber will be simplified as a hollow ball in the center of the optical fiber. The schematic diagram of the refraction loss is shown in Fig. 3, which is the meridian plane getting through the axis of optical fiber. In this schematic diagram, $n_{cl}(1.417)$ and $n_{co}(1.492)$ are the RIs of the fiber cladding and the fiber core, respectively, a and r are the radius of the fiber core and the micro-hole, respectively, α ($\approx 71.76°$) corresponding to the solid line is the critical angle at the core–cladding interface, and the corresponding incident angle and refraction angle at the interface of the hole are θ_1 and θ_2, respectively, in these critical conditions. We can see that the refraction beams of which the incident angle is smaller than the critical angle α at the core–cladding interface will be dissipated through the fiber cladding. For example, the light parallel to the axis of the optical fiber in the area between r_1 and r_2 will be lost after refraction of the micro-holes because the

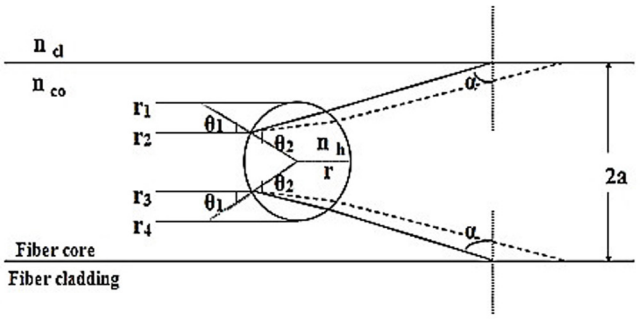

Fig. 3. Schematic diagram of refraction loss.

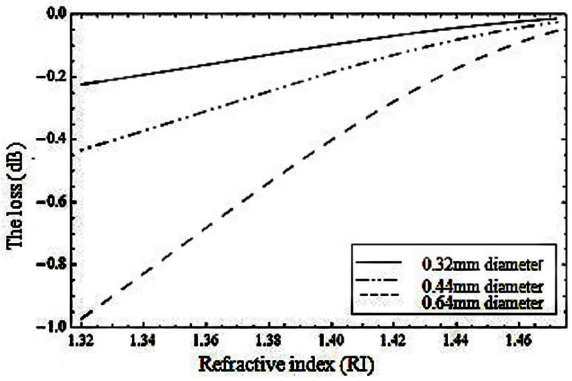

Fig. 4. Simulation curve of refraction loss.

incident angle at the core–cladding interface is smaller than the critical angle α. Similarly, the light between r_3 and r_4 will be lost as well. According to Snell's law, when n_h increases, the incident angle of some light that passes the hole will be larger than the critical angle at core–cladding interface, as shown by the dotted line, more ergo beams will be bounded in the fiber core and the output power of the fibers will increase. Because of the assumption that the transmission power in fiber cross-section is uniformly distributed and the numerical aperture (NA) of the fibers on both sides of the micro-holes are the same, we can substitute cross-sectional area of the optical pulse for light power, then the refraction loss of the fiber sensors can be deduced as

$$Lf_1 = 10 \lg \frac{a^2 - 4r^2 \cos^2 \theta_1}{a^2}. \tag{1}$$

Lf_1 is representative of the refraction loss of the fiber sensors and θ_1 meets the refraction law as

$$\theta_1 = \theta_2 - \pi/4 + \alpha/2, \tag{2}$$

$$n_{co} \sin\theta_1 = n_h \sin\theta_2. \tag{3}$$

From Eq. (1) we can get the simulation curve of the refraction loss of the sensors, as shown in Fig. 4. We can see that the sensitivity of the fiber sensors increases along with the increase in RI of the holes, the sensor with the largest micro-hole has the highest sensitivity. Increasing the diameter of the micro-holes increases the sensitivity of the sensor, and the loss of the fiber sensors will be close to zero in the condition that the RI of the liquid in the micro-hole is close to the RI of the fiber core.

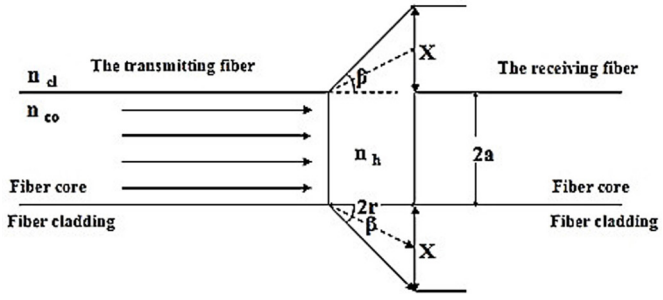

Fig. 5. Simulation curve of refraction loss.

Next, we will analyze the connection loss which is caused by the gap of the holes. The schematic diagram is shown in Fig. 5. The aperture of the two fibers is $2r$, which corresponds to the diameter of the micro-hole. The angle β is the maximum injection angle corresponding to the optical fiber NA (NA = 0.467), and is also the maximum divergence angle; it is determined by the core–cladding RI distribution and the RI of the receiving medium in the hole. X is the height of the leaky light projection area at the port of the receiving fiber. Their relations are as

$$\text{Sin} \quad \frac{\text{NA}}{}, \tag{4}$$

$$X = 2r \tan\beta. \tag{5}$$

The connection loss is determined by the projection area of the leaky beam, which is related to X and will become larger as X increases. Therefore, the connection loss is dependent on the value of X. As can be seen in Fig. 5, the beam (i.e., the dotted lines) will have a divergence angle between 0 and β and will be dissipated through the projection area with a certain height value of X. If n_h is increased, the angle β and the height X will decrease according to Eqs. (4) and (5), and reduce leakage at the aperture. Consequently, more of the beam will be guided into the fiber and the output power will increase. Similar to the mechanism of refraction loss, we can also substitute cross-sectional area of the optical pulse for the light power. The connection loss[24] of the fiber sensors can be deduced as

$$Lf_2 = 10 \lg \frac{\pi a^2}{\pi a^2 + 2(2r)^2 \tan\beta}. \tag{6}$$

Lf_2 shows that the connection loss of the fiber sensors is caused only by the micro-hole. Based on Eq. (6), Fig. 6 plots the simulation curve of the connection loss and shows that the loss and sensitivity of the fiber sensors will increase with the hole diameters in the fibers.

Aggregating the simulation curves for refraction loss (Fig. 4) and the connection loss (Fig. 6) will give the simulation curve for the total loss of the liquid RI sensors, as shown in Fig. 7. From this we can see that

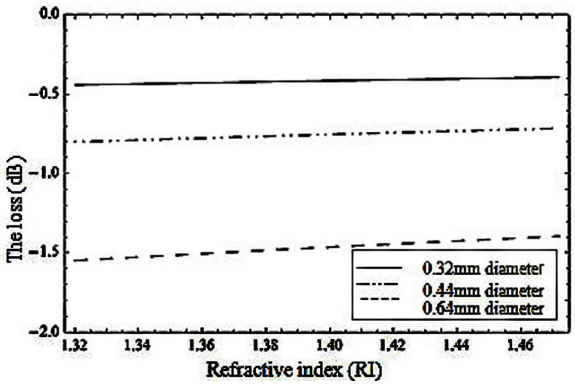

Fig. 6. Simulation curve of connection loss.

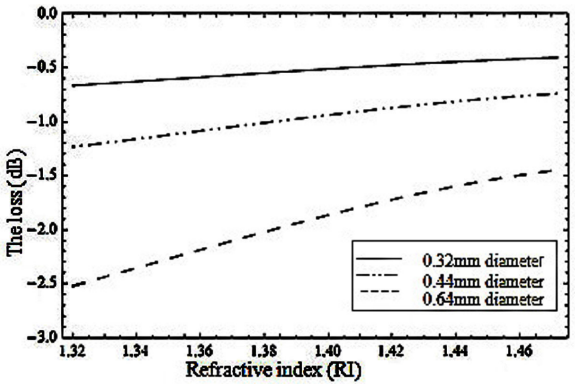

Fig. 7. Simulation curve of total loss of the liquid RI sensor.

the simulation results of the liquid RI fiber sensors are largely consistent with the experiment result. However, we can also see that the experimental value of the sensors have a higher loss compared with the theoretical value of Fig. 2. This can be explained with two reasons. Firstly, we only considered the fiber loss caused by the meridional rays running parallel to the axis and neglected the rays having other incident angles. Secondly, the effective area receiving light waves at the back of the micro-hole is smaller than the theoretical value, which is the cross-section of the fiber because of the existence of the micro-hole.

In conclusion, we demonstrate a simple and low-cost RI sensor based on step-index multimode POF with a micro-hole fabricated directly by femtosecond laser. The experiment uses the fibers with micro-holes of 0.32, 0.44, and 0.64 mm diameters, respectively, as the sensing fibers. All of the fiber sensors have a good linear dB response to the liquid RI in the holes and the sensitivity of the fiber sensors increases with the hole diameters. The fiber sensor with the largest micro-hole of 0.64 mm diameters demonstrates the highest sensitivity. Moreover, in a large operation RI range of 1.333–1.473, the sensitivity of the sensors can reach about 18 dB/RIU. A modeling of the sensing mechanism is developed as well from the refraction loss and connection loss. We calculate the simulated result and determined that it is largely consistent with the experimental result. The sensor discussed here has many advantages including designing simplicity, high sensitivity, and low cost and is suitable for applications in industries for liquid RI and quasi-distributed level measurement in hazardous regions.

References

1. G. Xin, K. Peng, Z. Gu, J. Zhao, R. Fan, L. Liu, and X. Xu, Chin. Opt. Lett. **11,** 020601 (2013).
2. P. M. Sandeep, S. W. B. Rajeev, M. Sheeba, S. G. Bhat, and V. P. N. Nampoori, Laser. Phys. Lett. **4,** 611 (2007).
3. M. V. Alfimov and A. M. Zheltikov, Laser. Phys. Lett. **4,** 363 (2007).
4. Y. Yu, L. Jiang, B. Li, Z. Cao, and S. Wang, Chin. Opt. Lett. **11,** 110603 (2013).
5. Q. Liu and Q. Wang, Chin. Opt. Lett. **10,** 090601 (2012).
6. C. Bariain, I. R. Matas, I. Romeo, J. Garrido, and M. Laguna, Appl. Phys. Lett. **77,** 2274 (2000).
7. A. Banerjee, S. Mukherjee, R. K. Verma, B. Jana, T. K. Khan, M. Chakroborty, R. Das, S. Biswas, A. Saxena, V. Singh, R. M. Hallen, R. S. Rajput, P. Tewari, S. Kumar, V. Saxena, A. K. Ghosh, J. John, and P. Gupta-Bhaya, Sens. Actuators B **123,** 594 (2007).
8. T. Zhu, Y. Rao, and Q. Mo, IEEE Photon. Technol. Lett. **17,** 2700 (2005).
9. V. Bhatia and A. M. Vengsarkar, Opt. Lett. **21,** 692 (1996).
10. X. W. Shu, L. Zhang, and I. Bennion, IEEE J. Lightwave Technol. **20,** 255 (2002).
11. Z. L. Ran, Y. J. Rao, J. Zhang, Z. W. Liu, and B. Xu, IEEE J. Lightwave Technol. **27,** 5426 (2009).
12. Y. Wang, D. N. Wang, M. W. Yang, W. Hong, and P. X. Lu, Opt. Lett. **34,** 3328 (2009).
13. Y. Lai, K. Zhou, L. Zhang, and I. Bennion, Opt. Lett. **31,** 2559 (2006).
14. Z. L. Ran, Y. J. Rao, W. J. Liu, X. Liao, and K. S. Chiang, Opt. Express **16,** 2252 (2008).
15. Y. Gong, T. Zhao, Y. J. Rao, Y. Wu, and Y. Guo, Opt. Express **18,** 15844 (2010).
16. T. Zhao, Y. Gong, Y. Rao, Y. Wu, Z. Ran, and H. Wu, Chin. Opt. Lett. **9,** 050602 (2011).
17. H. A. Rahman, S. W. Harun, M. Yasin, S. W. Phang, S. S. A. Damanhuri, H. Arof, and H. Ahmad, Sens. Actuators A **171,** 219 (2011).
18. T. L. Yeo, T. Sun, and K. T. V. Grattan, Sens. Actuators A **144,** 280 (2008).
19. L. Bilro, N. J. Alberto, L. M. Sa, J. L. Pinto, and R. Nogueira, J. Lightwave Technol. **29,** 864 (2011).
20. A. Armin, M. Soltanolkotabi, and P. Feizollah, Sens. Actuators A **165,** 181 (2011).
21. A. Martinez, M. Dubov, L. Y. Khrushchev, and L. Bennion, Mater. Res. Soc. Symp. Proc. **850,** MM2.3.1 (2004).
22. A. Kaur, S. E. Watkins, J. Huang, L. Yuan, and H. Xiao, Opt. Eng. **53,** 017105 (2014).
23. Y. N. Zhang, L. Yuan, X. W. Lan, A. Kaur, J. Huang, and H. Xiao, Opt. Lett. **38,** 4609 (2013).
24. T. C. Chu and A. R. McCormick, Bell Syst. Tech. J. **57,** 595 (1978).